Texture Anisotropy of the Brain's White Matter as Revealed by Anatomical MRI

Vassili Kovalev and Frithjof Kruggel*

***Abstract*—The purpose of this work was to study specific texture properties of the brain's white matter (WM) based on conventional high-resolution T_1-weighted magnetic resonance imaging (MRI) datasets. Quantitative parameters anisotropy and laminarity were derived from 3-D texture analysis. Differences in WM texture associated with gender were evaluated on an age-matched sample of 210 young healthy subjects (mean age 24.8, SD 3.97 years, 103 males and 107 females). Changes of WM texture with age were studied using 112 MRI-T_1 datasets of healthy subjects aged 16 to 70 years (57 males and 55 females). Both texture measures indicated a "more regular" WM structure in females ($p < 10^{-6}$). An age-related deterioration of WM structure manifests itself as a remarkable decline of both parameters ($p < 10^{-6}$) that is more prominent in females ($p < 10^{-6}$) than in males ($p = 0.02$). Texture analysis of anatomical MRI-T_1 brain datasets provides quantitative information about macroscopic WM characteristics and helps discriminating between normal and pathological aging.**

***Index Terms*—Age, anisotropy, gender, magnetic resonance imaging (MRI), texture, white matter (WM).**

I. Introduction

MACROSCOPIC-ANATOMICAL descriptions of the human brain are acquired by magnetic resonance imaging (MRI) within minutes today. A computer-based analysis of these imaging data leads to a quantitative characterization of structures, tissues, and their changes with time. The resulting extensive parameter sets are used in further statistical studies, e.g., to classify brains, to draw conclusions about structural differences in subject groups (i.e., by gender, structural abnormalities), and to track individual changes with time (aging, diseases of the central nervous system (CNS), therapeutical interventions).

One of the crucial tasks here is to define what is considered as "normal" or "pathological." Compared with the still valid gold standard—brain section—digital analysis methods offer the advantage of studying large population groups at different ages and *in vivo*. For successfully introducing computer vision methods in a clinical setting, they have to demonstrate their robustness against varying scanner properties (i.e., changes in intensity, contrast, and noise), and their ability to detect pathological changes at a well-documented sensitivity level.

Manuscript received October 27, 2006; revised January 15, 2007. This research was supported by the fellowship program of the Max-Planck Society, Germany. *Asterisk indicates corresponding author.*

V. Kovalev is with the United Institute of Informatics Problems, Belarus National Academy of Sciences, 220012 Minsk, Belarus, (e-mail: vassili.kovalev@gmail.com

*F. Kruggel is with the University of California at Irvine, Irvine, CA 92697-2755 USA (e-mail: fkruggel@uci.edu).

Digital Object Identifier 10.1109/TMI.2007.895481

Texture features provide integral, quantitative information about structural properties at a millimeter scale. We recently demonstrated that the characterization of tissue properties by 3-D volumetric texture analysis [1], [2] is robust and is highly sensitive for detecting image features that may be related to degeneration or attributed as pathological signs. The purpose of this work was to introduce texture anisotropy and laminarity as neurobiologically interesting parameters that describe properties of the brain's white matter (WM) as revealed by high-resolution T_1-weighted MRI. These image-based parameters may reflect WM tissue properties such as the local coherence, direction and density of fiber bundles, their myelinisation status, the density and direction of vessels supplying and draining the WM, and findings commonly associated with aging (e.g., lacunes, enlarged periventricular spaces). We tested for age-related changes and gender-related differences of these WM texture measures in a reasonably large population sample. Extreme cases in terms of the statistic may be considered as pathological.

The concept of generalized co-occurrence matrices was introduced in [3], and texture anisotropy measures in 3-D were evaluated first in [4] and recast in a common framework in [2]. As a neurobiological example application, we studied the macrostructural asymmetry of the human brain in the same sample [5].

It is important to note that despite an immediate terminological association, our texture anisotropy, as measured here on T_1-weighted images, does not necessarily relate to the anisotropy measures obtained from diffusion tensor imaging [6]–[8].

II. Materials and Methods

A. Subjects

This study relies on a database of subjects enrolled for functional MRI experiment. Before admission, a brief history and physical examination is taken by a physician, and a high-resolution T_1-weighted MRI scan of the head is acquired. Subjects are included in this database if they comply with the informed consent for conducting general fMRI experiments, pass the examination, and do not exhibit pathological or abnormal features (such as ventricular enlargements, subarachnoidal cysts) in their MRIs. The WM anisotropy differences associated with gender were evaluated using a group GEN consisting of 210 young healthy subjects [mean age 24.8, standard deviation (SD) 3.97 years] including 103 males (mean age 25.3 years, SD 3.94) and 107 females (mean age 24.3 years, SD 3.97) with insignificant age difference. Changes of WM anisotropy with age were studied using a group AGE of

112 healthy subjects from the same database (57 males and 55 females) aged 16 to 70 years. Subjects were selected to include approximately three per year of age and balanced for gender. Both GEN and AGE groups were selected prior to the analyses.

B. Image Data

MRI acquisition was performed on a Bruker 3T Medspec 100 system equipped with a bird cage quadrature coil using a T_1-weighted 3-D modified driven equilibrium Fourier transform (MDEFT) protocol [9]: field-of-view (FOV) $240 \times 240 \times 192$ mm, matrix 256×256, TR $=$ 1.3 s, TE $=$ 10 ms, 128 sagittal slices, voxel size 0.9×0.9 mm, 1.5-mm slice thickness, scanning time 15 min. Acquired data were interpolated to an isotropical voxel size of 1.0 mm and aligned with the stereotactical coordinate system by applying a rigid transformation using a fourth-order b-spline method for interpolation [10] while removing the outer hulls of the brain [11]. Data were corrected for intensity inhomogeneities by a fuzzy segmentation approach using three classes [12], yielding an intensity-corrected T_1-weighted image, and a set of probability images. Only voxels in Class 2 with $p > 0.65$ were taken into account as a mask of the WM compartment. Datasets were finally cropped to a minimum box enclosing the brain of $160 \times 200 \times 160$ mm extent. Image analysis methods were implemented in the C programming language for recent PC workstations. Statistical analyses were performed using the STATISTICA 5.0 software package.

C. Measuring Texture Anisotropy

Three-dimensional anisotropy histograms [1], [4] and gradient angle co-occurrence matrices [2] were used to evaluate the anisotropy properties of WM texture. Both techniques use the orientation of MRI-T_1 intensity gradient vectors computed over all WM voxels. Gradient vectors are calculated in a voxel neighborhood and normalized to unit vectors so that only information about the directionality (vector angles) is considered.

For the first technique, all possible 3-D directions are quantified to equal solid angle bins and vectors falling into each bin are counted. Such anisotropy histograms can be visualized as 3-D graphs, in which the radius in a specific direction is proportional to the number of gradient vectors identified in this direction. If image data were fully isotropic, all bins would be equally populated and the graph would correspond to a sphere. Thus, the anisotropy of WM texture can be measured as the amount of deviation from this ideal histogram. The second approach considers adjacent voxel pairs that are assessed for their relative orientation. The measure corresponding to this local coherence of gradient vectors is defined as laminarity and roughly understood as the relative amount of WM tissue with a nearly parallel grayscale pattern (see Fig. 1).

D. Anisotropy Measure

Three issues are considered when computing anisotropy: the "binning" of the gradient orientation (tessellation of the unit sphere), the selection of a suitable way for calculating gradient vectors, and the definition of the anisotropy feature.

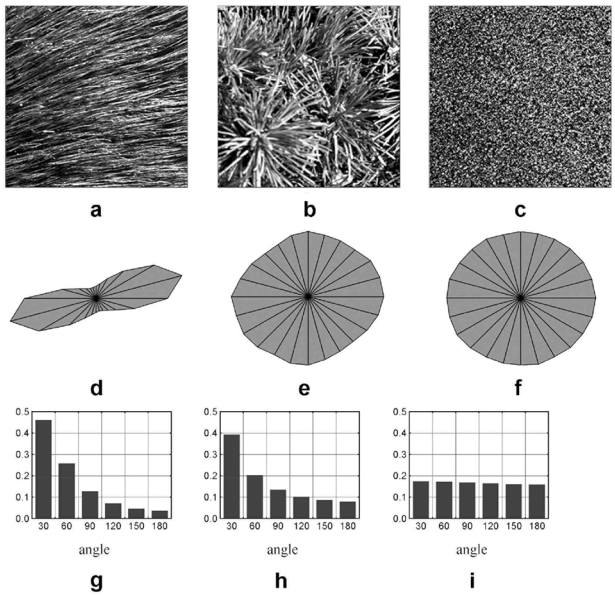

Fig. 1. Example of natural textures (upper row) and their anisotropy (middle row) and laminarity (bottom row) properties. (a) Anisotropic, laminar texture ($A = 20.3, L = 0.460$). (b) Isotropic, laminar texture ($A = 1.92, L = 0.393$). (c) Isotropic, nonlaminar texture ($A = 1.13, L = 0.175$).

Tessellation of the Unit Sphere: We quantize gradient directions in three dimensions into equal solid angles which corresponds to tessellating the sphere's surface into equal-sized patches. A point on the unit sphere is defined in terms of longitude ϕ measured along the equator and the elevation z above the equatorial plane. Patches are defined by dividing ϕ and z in equally sized intervals of equal area. Dividing $0 \leq \phi < 360°$ into M equal intervals and $-1 \leq z \leq 1$ in N equal segments results in $(N-2) \times M$ spherical quadrangles and $2M$ spherical triangles (on poles), all sustaining the same solid angle of $4\pi/(NM)$. An arbitrary direction defined by vector (a, b, c) belongs to the anisotropy histogram bin $h(m, n)$ if the following two conditions are met:

$$\frac{2\pi}{M} m \leq \phi < \frac{2\pi}{M}(m+1)$$

where

$$\sin\phi = \frac{b}{\sqrt{a^2+b^2}}, \quad \cos\phi = \frac{a}{\sqrt{a^2+b^2}},$$

$$-1 + \frac{2}{\pi} n \leq \bar{c} < -1 + \frac{2}{\pi}(n+1)$$

where

$$\bar{c} = \frac{c}{\sqrt{a^2+b^2+c^2}}.$$

Here, $M = 24$ and $N = 13$ were found as a good compromise between the resolution (sensitivity) of anisotropy histograms and robustness of resulting features (see also [4]).

Calculating Gradient Vectors and Anisotropy Histograms: We visit every WM voxel i and compute components $G_x(i), G_y(i)$, and $G_z(i)$ of its gradient vector $G(i)$ by convolving the $3 \times 3 \times 3$ image neighborhood with the orthogonal masks of a 3-D Zucker–Hummel filter [13]. Only voxels

belonging to the WM class were included in the computation of the gradients. The unit gradient vector $g(i)$ with components $g_x(i), g_y(i)$, and $g_z(i)$ is obtained by dividing the components $G_x(i), G_y(i)$, and $G_z(i)$ by the intensity gradient magnitude $\sqrt{G_x^2 + G_y^2 + G_z^2}$. This normalization particularly achieves the insensitivity of unit vectors to the original intensity scale.

For calculating the anisotropy histogram $H = ||h(m,n)||$ with the angle bins $h(m,n)$, we identify the bin using both conditions given above. Thus, the anisotropy histogram counts only the number of the unit vectors oriented in a given direction irrespective of the magnitude of intensity variation. Due to random noise, gradient vectors with small magnitudes (e.g., <5% of the maximum value) have poorly defined orientations. In our experience, leaving out results from these voxels (typically about 0.05%) increases the robustness of anisotropy measurements [1]. Finally, the anisotropy histogram is normalized by the sum of bins to avoid a dependence on the number of visited voxels.

Anisotropy Feature: In principle, the whole anisotropy histogram can be used to represent the texture anisotropy. Ideally, one would prefer to use only a few parameters to represent this feature. A rather global characteristic is the deviation of a particular histogram from the histogram of an ideally spherical distribution that implies a totally isotropic volume. Thus, anisotropy is defined here as [1]

$$A = \sqrt{\frac{1}{NM}\sum_{n=1}^{N}\sum_{m=1}^{M}(h(m,n) - \bar{h})^2}$$

where $h(m,n)$ denotes the value of the anisotropy histogram bin (m,n) and $\bar{h}$ is the mean histogram value. The anisotropy feature A expresses the degree of anisotropy of a texture measured as the standard deviation of the distribution of gradient vector orientations in 3-D.

E. Laminarity Measure

A complementary way to characterize anisotropic properties of anatomical brain datasets is based on so-called gradient angle co-occurrence matrices [2]. These matrices and a derived quantitative measure, referred to as laminarity here, are described below.

Gradient Angle Co-Occurrence Matrices: The gradient angle co-occurrence matrix is a 2-D array that represents the frequency of spatial occurrence of voxel pairs with a certain relative orientation of their gradient vectors at a given range of intervoxel distances. Consider an arbitrary voxel pair (i,k) defined on discrete voxel lattice by indexes $i = (x_i, y_i, z_i)$ and $k = (x_k, y_k, z_k)$ at a Euclidean distance $d(i,k)$. Denote the angle between their 3-D gradient vectors by $a(i,k)$. The gradient angle co-occurrence matrix is defined as

$$W = (w(d(i,k), a(i,k)))$$

where

$$a(i,k) = \cos^{-1}(g(i) \cdot g(k))$$

and w is the number of WM voxel pairs (i,k) at the given distance $d(i,k)$. The angle between gradient vectors $a(i,k)$ is computed from the dot vector product of the normalized intensity gradient vectors $g(i), g(k)$ obtained above. All possible voxel pairs inside the WM mask with no repetition are considered when calculating the matrix. Using normalized gradient vectors provides insensitivity of matrices to image intensity. Normalization by the sum of voxel pairs yields volume independence. Anisotropy descriptors are rotation/reflection invariant because they take only the relative gradient orientation into account.

Laminarity Feature: Gradient angle co-occurrence matrices provide a detailed description of the orientational structure of 3-D textures. In a prestudy, their discrimination abilities were evaluated on more than 300 brain datasets with 1-mm^3 voxel resolution. We determined an optimal angle bin size of 30° (six bins for the whole range of 180°). Considering intervoxel distances greater than 2 mm did not provide statistically significant benefits due to the high spatial frequency of brain WM texture and relatively fast decline of the autocorrelation function. Hence, it is sufficient to limit intervoxel distances to one raster unit $(d(i,k) = 1)$, so the 2-D co-occurrence matrix collapses to its first row. The first element $w(1,1)$ measures the relative amount of voxel pairs with relative gradient angles of 0°–30°, the second element $w(1,2)$ counts pairs with angles 30°–60°, and so on. Thus, for a perfectly laminar texture formed by locally parallel structures (e.g., "layers," "stripes," "tubes"), all voxel pairs fall into the first bin $(w(1,1) = 1)$ while other bins are empty. Thus, we define the laminarity feature L as the value of the first element of the gradient angle co-occurrence matrix: $L \equiv w(1,1)$. At a spatial resolution of 1 mm, the intervoxel distance of one raster unit corresponds to the physical distances between 1.0 and 1.73 mm with an average of 1.42 mm. The laminarity L is robust because it is an average value by nature and sampled over a typical number of 1.8×10^6 voxel pairs.

The laminarity feature L may roughly be understood as the relative WM volume with a nearly laminar structures (angle less than 30°) measured at the scale of 1.42 mm.

F. Comparison of Anisotropy and Laminarity Features

Anisotropy describes the global, dominant directionality of WM tissue by summing up local orientations over the solid angle bins with predefined directions relative to the image coordinate frame. The laminarity feature measures the local spatial coherence and, therefore, it is insensitive to the global shape of the WM compartment.

Differences are illustrated in Fig. 1 with test images representing natural grayscale textures of three basic classes: anisotropic, laminar [Fig. 1(a)], isotropic, laminar [Fig. 1(b)], and isotropic, nonlaminar [Fig. 1(c)]. Anisotropic properties of these textures are depicted as histograms in Fig. 1, middle. For this illustrative experiment, original 2-D images were converted to pseudovolumetric datasets with three identical slices. Thus, there is no intensity variation along the z-axis and 3-D anisotropy histograms are flat. Note also that the dominant direction of anisotropy histogram is perpendicular to the actual texture direction by definition. The bottom row of Fig. 1 shows the 1-D gradient angle co-occurrence histograms, the first column of which expresses the laminarity degree of each test

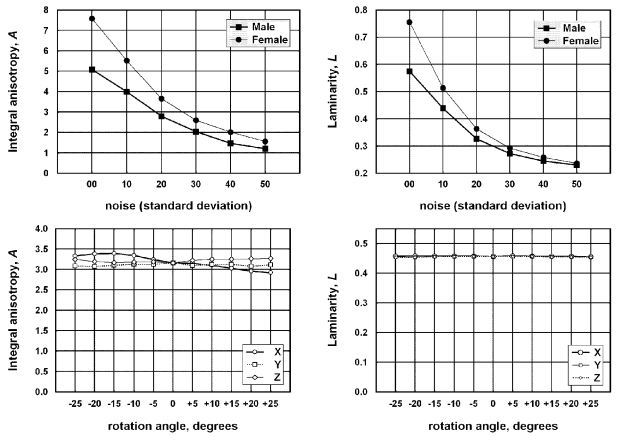

Fig. 2. Top: Dependence of noise levels with standard deviation of 0–50 units for anisotropy (left) and laminarity (right). Adding noise detoriates texture properties, resulting in a strong decline of measures with increasing noise levels. Gender differences become small but never change sign. Below: Dependence of anisotropy on rotation angles between -25° and 25°. Anisotropy is almost independent of rotation in y- and z-direction (front-to-back resp. body axis), while there is a noticable decrease with rotation in x-direction. The laminarity measure is independent of rotation.

image. Corresponding quantitative values of the anisotropy and laminarity are given in the figure caption. Note that the minimum possible laminarity of natural textures is $1/N$ (uniform distribution), or $1/6 = 0.167$ in this study. Anisotropy and laminarity are correlated for most textures except for those similar to Fig. 1(b).

III. Results

A. Evaluation

To evaluate properties of our texture measures, we examined their stability against 1) noise, 2) intensity inhomogeneities, 3) scaling, and 4) rotation using simulated influences on real datasets. Note that our datasets have 256 intensity levels.

Noise: The level of random (Gaussian) noise obviously influences texture measures. We arbitrarily selected datasets of a male (25.7 years old) and a female (22.4 years old) subject. Gaussian noise was added to these datasets with a standard deviation of {0, 10, 20, 30, 40, 50} units, compared with an average noise level of 6 in our data. Results are shown in Fig. 2, top. As expected, adding noise detoriates texture properties, resulting in a strong decline of measures with increasing noise levels. For unrealisticly high noise levels, gender differences become small but never change sign. We conclude that higher noise levels disturb regular texture and decrease gender-related effects.

Intensity Inhomogeneities: A linear multiplicative intensity gradient in the x-direction (ear-to-ear) and y-direction (front-to-back) was applied to both datasets above with a slope of {0, 0.25, 0.50, 0.75, 1.00, 1.25, 1.50} units/voxel. Laminarity (as a local measure) showed very little change (less than 5%) even with very strong intensity inhomogeneities, while anisotropy (as a global measure) increases with a stronger intensity gradient (about 60%). Gender differences remained almost constant with increasing intensity inhomogeneities. In our original data, intensity inhomogeneities of about 15%–20% (peak-to-peak) are typical, and partially corrected for by the post-hoc correction scheme referenced above. This corresponds to a slope of 0.50 units/voxel in our simulation experiment. We conclude that intensity inhomogeneities affect anisotropy, but not laminarity values. No interaction with gender was found.

Scaling: A single dataset was linearly scaled in all three dimensions by a factor of {0.85, 0.90, 0.95, 1.00, 1.05, 1.10, 1.15}, roughly corresponding to the natural variation in brain size. Laminarity slightly increased with scaling by 12% over the range studied here. Downscaling a regular texture leads to an increase of intervoxel distance and to more randomly oriented gradient vector, and thus, to higher laminarity values. Anisotropy decreases slightly with upscaling (by 5%), but more strongly with downscaling (by 20%). With "compression" of neighboring voxels, gradients are higher in magnitude and more unstable in direction.

Rotation: A single dataset was rotated in all three dimensions by {−25, −20, −15, −10, −5, 0, 5, 10, 15, 20, 25} degrees. Results are shown in Fig. 2, bottom. The anisotropy measure is almost independent of rotation in y- and z-direction (body axis), while there is a noticable decrease with rotation in the x-direction. Laminarity measures local, relative gradient orientation and is independent of rotation.

To summarize, the influence of noise, intensity inhomogeneities, scaling, and rotation on the values of our texture measures may be well understood and explained from their definition.

TABLE I
Gender-Related Differences of WM Texture Measures (Anisotropy A and Laminarity L) in Young Subjects (Group GEN). Codes for P-Values Are: $0 \leq *** < 0.001$

Compartment	Feature	Mean male	Mean female	Significance $z-$score	Significance $p-$value
Brain	A	2.92	3.26	3.70	***
	L	0.453	0.479	6.59	***
Left	A	3.28	3.65	3.41	***
Hemisphere	L	0.462	0.485	5.39	***
Right	A	3.18	3.58	3.22	**
Hemisphere	L	0.445	0.475	7.17	***

B. Gender-Related Differences in WM Texture Measures

The differences of WM texture anisotropy associated with gender were evaluated based on 210 MRI-T_1 datasets of young healthy controls (group GEN, 103 males and 107 age-matched females). Anisotropy A and laminarity L were computed for the whole WM and for both hemispheric compartments. Group differences were evaluated by linear regression using gender and brain volume as factors. Results are summarized in Table I and interpreted as follows.

1) WM texture anisotropy and laminarity are significantly different for male and female subgroups. WM in males is consistently less laminar (more disordered) and more isotropic than in females.
2) Gender-related differences in WM anisotropy are approximately similar for the whole brain and brain hemispheres.
3) Laminarity shows a higher discrimination power than anisotropy.

TABLE II
DIFFERENCES OF WM TEXTURE MEASURES (ANISOTROPY A AND LAMINARITY L) IN SUBJECT PAIRS MATCHED FOR AGE AND BRAIN VOLUME. CODES FOR P-VALUES ARE: $0 \leq *** < 0.001 \leq ** < 0.01 \leq * < 0.05$

Compartment	Feature	Mean male	Mean female	Significance $z-$score	Significance $p-$value
Brain	A	2.99	3.23	3.19	**
	L	0.457	0.477	5.05	***
Left	A	3.35	3.63	3.05	**
Hemisphere	L	0.466	0.482	4.11	***
Right	A	3.29	3.53	2.49	*
Hemisphere	L	0.448	0.472	5.50	***

TABLE III
MULTIPLE REGRESSION OF WM TEXTURE MEASURES (ANISOTROPY A AND LAMINARITY L) WITH AGE AND GENDER IN GROUP AGE. CODES FOR P-VALUES ARE: $0 \leq *** < 0.001, 0.1 \leq - \leq 1$

Compartment	Feature	Age regression coefficient	Age z score	Age p value
Brain	A	-0.0200	-5.94	***
	L	-9.85e-4	-6.30	***
Left	A	-0.0219	-5.62	***
Hemisphere	L	-9.43e-4	-6.05	***
Right	A	-0.0210	-5.75	***
Hemisphere	L	-1.01e-3	-5.93	***

Compartment	Feature	Gender regression coefficient	Gender z score	Gender p value
Brain	A	0.0612	0.698	-
	L	0.0176	4.19	***
Left	A	0.0576	0.558	-
Hemisphere	L	0.0157	3.72	***
Right	A	0.0570	0.605	-
Hemisphere	L	0.0208	4.53	***

The influence of brain volume on the texture measures is small but statistically significant: lower anisotropy and laminarity values were found in larger brains. To prove that gender-related differences are not just attributed to size differences, we selected 57 pairs of male/female subjects with a pairwise difference in brain size of less than 1% that is statistically insignificant ($p = 0.980$). A pairwise t-test was used to evaluate gender differences of texture measures. Results are compiled in Table II.

Comparing results in Tables I and II, we conclude that gender-related differences in our texture measures remain highly significant.

C. Changes of WM Texture Measures With Age

Changes of anisotropy and laminarity with age were evaluated in group AGE of 112 subjects over a life span of 16 to 70 years. Linear regression with factors age, gender, and brain volume was used, and results are summarized in Table III.

A highly significant decline of WM texture measures with age was found for both measures. Evaluating texture measures for the whole brain compartment separately for females and males, a stronger decline for females is determined for anisotropy (-0.0223 versus -0.0175) and for laminarity (-1.22×10^{-3} versus -7.45×10^{-4}) (see also Fig. 3). This

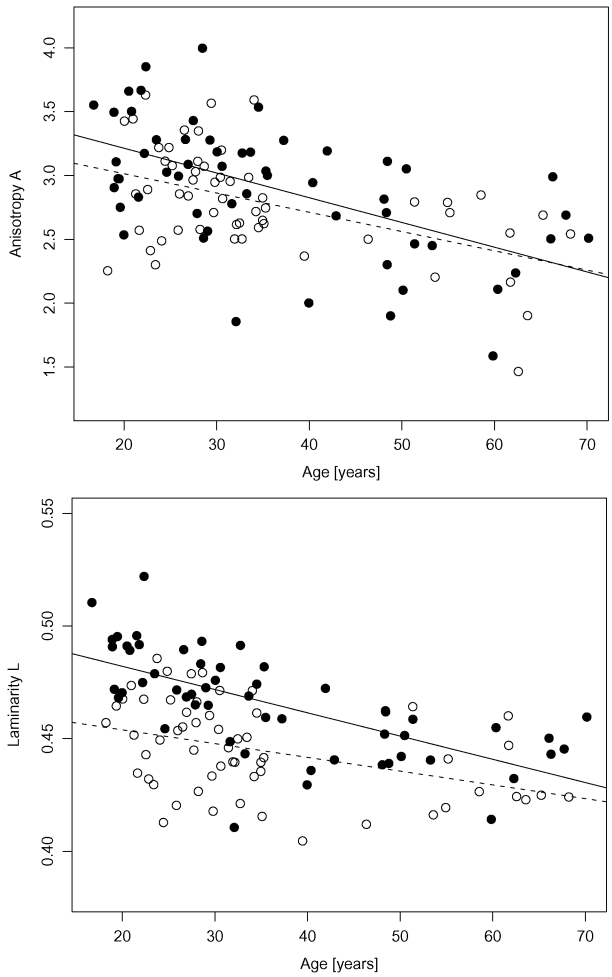

Fig. 3. Changes of WM anisotropy (top) and laminarity (bottom) with age (group AGE, 112 subjects). Filled circles correspond to values of females, open circles to males. The regression line shows a stronger decline for females (solid) than for males (dashed) for both parameters. Over the age range examined here, gender differences become insignificant for the anisotropy measure, but remain significant for the laminarity measure.

stronger decline renders gender differences in anisotropy insignificant over the life span included here, while differences remain significant for laminarity.

Fig. 4 provides examples of two extreme datasets with visually evident differences in WM structure along with their 3-D anisotropy histograms. It can be clearly seen that the histogram of the second dataset with the lowest texture anisotropy (higher WM disorder) has more a spherical shape than the first one.

IV. DISCUSSION

A. Main Findings

We summarize the main findings of this study as follows.

1) There are significant differences in WM texture associated with gender. In young females, both anisotropy and laminarity are consistently higher than in young males, corresponding to a more laminar and less disordered texture.
2) A highly significant decline of anisotropy and laminarity with age was found, and interpreted as an age-related deterioration of spatially directed WM structures (e.g., fiber

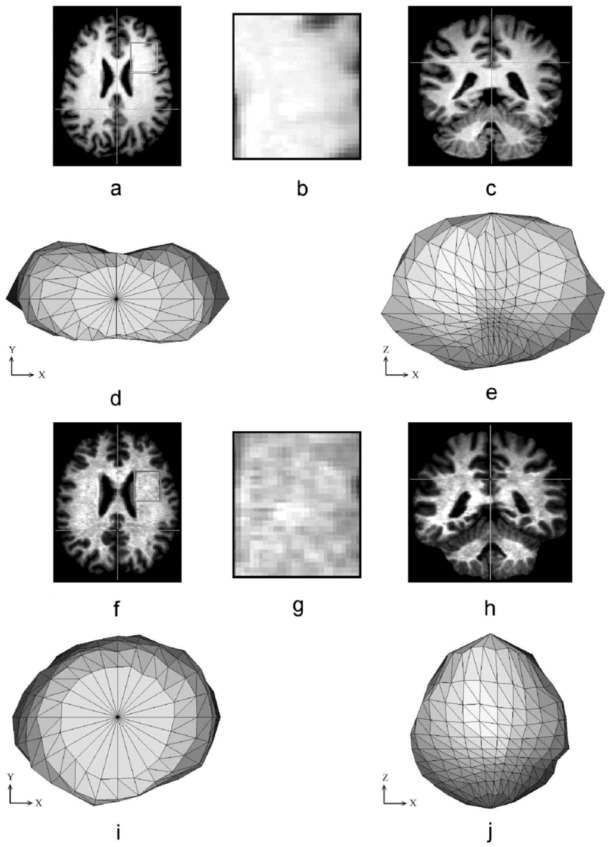

Fig. 4. Two sample subjects from group AGE with high (top) and low (bottom) WM texture anisotropy. (a)–(c) Axial and coronal slices of Subject 1 (female, 22 years old, $A = 3.85, L = 0.522$) and its WM anisotropy histogram viewed from the top (d) and back (e). (f)–(g) Axial and coronal slices of Subject 2 (male, 40 years old, $A = 2.37, L = 0.405$) and its WM anisotropy histogram viewed from the same positions in 3-D (i), (j). Close-ups (b) and (g) give a visual impression of the difference in WM texture. Image slices are contrast-enhanced; the GM compartment is kept for clarity.

bundles). This decline is more prominent in females than in males and renders gender-related differences insignificant for the anisotropy, but not for the laminarity measure.

3) WM texture parameters were similar in magnitude for the whole WM compartment and both hemispheres. Differences with gender and changes with age were similar for all compartments.

Laminarity is a very sensitive feature that captures both age and gender-related anisotropy changes. It is superior to anisotropy feature in all tests. Most likely, the better discriminative power of the laminarity feature can be explained by its insensitivity to global brain shape that varies considerably across subjects and blurs the anisotropy measures. As expected, both measures are correlated with a coefficient of 0.714 in group GEN and 0.656 in group AGE.

B. Reproducibility Notes

General findings reported with our study are expected to be easily reproducible on MRI-T_1 datasets using the image analysis methods described here. Nevertheless, the absolute values of WM texture parameters may depend on several technical details. Some important points that should be considered in similar studies are listed below.

Spatial Resolution: Images should be acquired at a high spatial resolution and an (almost) isotropical voxel size. Anisotropy values depend on the acquisition resolution since they measure texture directionality as presented by the imaging data. The resolution of our MRI-T_1 datasets was the same in all three axes with the interpolated voxel size of 1 mm^3. At a lower resolution, texture features may not be revealed due to the partial volume effect and greater intervoxel distances. For instance, measurement of WM laminarity in young subjects with $d = 2$ raster units results in smaller mean values: $L = 0.239$ for males and $L = 0.261$ for females while the original magnitudes are 0.453 and 0.479, respectively (see Table I). The nonuniformity artificially increases anisotropy in the direction of greater dimension of brick-shaped voxels. A nonuniform sampling can be handled by means of appropriate scaling of gradient components $G_x(i), G_y(i)$, and $G_z(i)$ when calculating gradient vector directions [4].

Image Acquisition: A number of technical factors related to properties of the MR apparatus and imaging protocol influence the value of descriptors derived from texture analysis [14]. While it was impossible to control for all factors in this retrospective analysis, the relative stability of texture measures with rotation, scaling, intensity inhomogeneity, and noise was documented in the experimental section. We argue that these technical factors are unlikely to exhibit a systematic influence explaining the age- and gender-related differences found here.

Note that all measurements were performed using the same imaging protocol run on the same 3.0 T scanner. A preliminary investigation revealed that the WM laminarity computed for datasets acquired using a different imaging protocol on a 1.5 T scanner are higher.

C. Relations With Previous Studies

This work focuses on the quantitative characterization of WM anisotropy as revealed by conventional T_1-weighted MR imaging using 3-D texture analysis methods. This approach has not previously been studied.

Structural WM changes associated with age and gender were examined by various methods, e.g., by evaluating gross volumetric differences [15]–[18], by investigating the deterioration of WM microstructure postmortem [19]–[21], and *in vivo* by MRI [8], [22]–[27], and diffusion-tensor imaging [6].

It is well documented that the gross WM volume is approximately constant until the fourth decade, and then declines with age [15], [17], [18]. [23], [25]. Several mechanisms may account for this finding. Histopathologic evidence shows that myelin breakdown progresses with age [28], and is considered a major factor in the age-related cognitive decline associated with aging [29]. It was hypothesized that myelin breakdown exceeds maturation in adults and exerts a constant factor throughout lifetime. Wallerian degeneration due to (cortical) neuronal loss is probably not explaining axonal myelin changes [30]. Pathologic changes in small blood vessels are associated with diffuse WM changes and may have a distinct role in the genesis of vascular dementia [31]. Mild signs of diffuse vacuolization and arteriolosclerosis are a common finding in elderly subjects and are likely to detectable as age-related changes of WM.

Recent evidence from comparing high field MR microscopic imaging and histopathology in multiple sclerosis lesions has demonstrated that myelin content and axonal density correlates strongly with T_1 relaxation time [21]. This effect offers an explanation for the age-related decrease of the gray matter (GM)/WM contrast in macroscopic T_1-weighted MRIs [24]. Similarly, changes in T_2 relaxation time show a strong correlation with age [22].

Diffusion tensor imaging is understood to measure the apparent local diffusion coefficient of extracellular water, as impeded by local microstructure (e.g., axons, microvessels). Results [6] demonstrated a significant decline of fractional WM anisotropy with age in the genu and splenium of the corpus callosum, the centrum semiovale, and the frontal and parietal pericallosal WM [26]. By assessing the normal brain development in neonates and infants [7], it was found that diffusional WM anisotropy is a sensitive indicator of brain maturation and it precedes an MRI-T_1 intensity change.

Texture properties are evaluated on a millimeter scale, and may capture the local coherence, direction, and density of fiber bundles, their myelinisation status, the density and direction of vessels supplying and draining the WM, and findings commonly associated with aging (e.g., lacunes, enlarged periventricular spaces). Our results are in accordance with similar findings obtained for specific brain structures on the micro level [8], [19], [26], [32].

A possible explanation for the gender-related differences documented here may be given when taking results of a separate study [5] into account. With a similar approach based on texture features, it was demonstrated that brain hemispheres are more symmetric in females than in males. Thus, a more symmetric brain allows for a more regular "wiring layout" of the WM compartment, which is equally true for long- and short-range connections. Hence, this hypothesized regular WM wiring layout in females corresponds to a higher texture anisotropy and greater laminarity of WM structures.

All subjects included in this study were apparently healthy, by report and by inspection. Any pathologic process (e.g., diffuse or focal WM lesions) is expected to disturb structural features and lead to a reduction of WM laminarity and anisotropy in comparison with an age-related population sample. Thus, texture measures may be of diagnostic relevance as a quantitative parameter describing local structural properties of the WM compartment.

In conclusion, this study demonstrated that the texture anisotropy analysis of anatomical MRI-T_1 brain datasets provides quantitative information, which may help to better understand the gender-related differences and WM alterations with brain maturation and aging.

ACKNOWLEDGMENT

Datasets were kindly provided by the Max-Planck Institute of Cognitive Neuroscience, Leipzig, Germany.

REFERENCES

[1] V. A. Kovalev and M. Petrou, "Texture analysis in three dimensions as a cue to medical diagnosis," in *Handbook of Medical Imaging: Processing and Analysis*, I. N. Bankman, Ed. San Diego, CA: Academic, 2000, pp. 231–247.

[2] V. A. Kovalev, F. Kruggel, H.-J. Gertz, and D. Y. von Cramon, "3-D texture analysis of MRI brain datasets," *IEEE Trans. Med. Imag.*, vol. 20, no. 5, pp. 424–433, May 2001.

[3] V. Kovalev and M. Petrou, "Multidimensional co-occurrence matrices for object recognition and matching," *Graph. Models Image Process.*, vol. 58, no. 3, pp. 187–197, 1996.

[4] V. A. Kovalev, M. Petrou, and Y. S. Bondar, "Texture anisotropy in 3-D images," *IEEE Trans. Image Process.*, vol. 8, no. 3, pp. 346–360, Mar. 1999.

[5] V. A. Kovalev, F. Kruggel, and D. Y. von Cramon, "Gender and age effects in structural brain asymmetry as measured by MRI texture analysis," *NeuroImage*, vol. 19, pp. 896–905, 2003.

[6] P. J. Basser, "Inferring microstructural features and the physiological state of tissues from diffusion-weighted images," *NMR Biomed.*, vol. 8, pp. 333–344, 1995.

[7] K. Takeda, Y. Nomura, H. Sakuma, T. Tagami, Y. Okuda, and T. Nakagawa, "MR assessment of normal brain development in neonates and infants: Comparative study of T1- and diffusion-weighted images," *J. Comput. Assisted Tomogr.*, vol. 21, pp. 1–7, 1997.

[8] A. Virta, A. Barnett, and C. Pierpaoli, "Visualizing and characterizing white matter fiber structure and architecture in the human pyramidal tract using diffusion tensor MRI," *Magn. Reson. Med.*, vol. 17, pp. 1121–1133, 1999.

[9] J. H. Lee, M. Garwood, R. Menon, G. Adriany, P. Andersen, C. L. Truwit, and K. Ugurbil, "High contrast and fast three-dimensional magnetic resonance imaging at high fields," *Magn. Reson. Med.*, vol. 34, pp. 308–312, 1995.

[10] P. Thevenaz, T. Blu, and M. Unser, "Image interpolation and resampling," in *Handbook of Medical Imaging: Processing and Analysis*, I. N. Bankman, Ed. San Diego, CA: Academic, 2000, pp. 393–420.

[11] F. Kruggel and D. Y. von Cramon, "Alignment of magnetic-resonance brain datasets with the stereotactical coordinate system," *Med. Image Anal.*, vol. 3, pp. 175–185, 1999.

[12] D. L. Pham and J. L. Prince, "Adaptive fuzzy segmentation of magnetic resonance images," *IEEE Trans. Med. Imag.*, vol. 18, no. 9, pp. 737–752, Sep. 1999.

[13] S. W. Zucker and R. A. Hummel, "A 3-D edge operator," *IEEE Trans. Pattern Anal. Mach. Intell.*, vol. 3, no. 3, pp. 324–331, May 1981.

[14] L. R. Schad, "Problems in texture analysis with magnetic resonance imaging," *Dialogues Clin. Neurosci.*, vol. 4, pp. 235–242, 2002.

[15] D. D. Blatter, E. D. Bigler, C. S. Johnson, C. Anderson, and S. D. Gale, "A normative database from magnetic resonance imaging," in *Neuroimaging I: Basic Science*, E. D. Bigler, Ed. New York: Plenum, 1996, pp. 79–95.

[16] C. D. Good, I. S. Johnsrude, J. Ashburner, R. N. A. Henson, K. J. Friston, and R. S. J. Frackowiak, "A voxel-based morphometric study of aging in 465 normal adult human brains," *NeuroImage*, vol. 14, pp. 21–36, 2001.

[17] C. R. Guttmann, F. A. Jolesz, R. Kikinis, R. J. Killiany, M. B. Moss, T. Sandor, and M. S. Albert, "White matter changes with normal aging," *Neurology*, vol. 50, pp. 972–978, 1998.

[18] W. Meier-Runge, J. Ulrich, M. Bruehlmann, and E. Meier, "Age-related white matter atrophy in the human brain," *Ann. New York Acad. Sci.*, vol. 673, pp. 260–269, 1992.

[19] F. Aboitz, E. Rodrigues, R. Olivares, and E. Zaidel, "Age-related changes in fiber composition of the human corpus callosum: Sex differences," *Neuroreport*, vol. 7, pp. 1761–1764, 1996.

[20] Y. Tang, J. R. Nyengaard, B. Pakkenberg, and H. J. G. Gundersen, "Age-induced white matter changes in the human brain: A stereological investigation," *Neurobiol. Aging*, vol. 18, pp. 609–615, 1997.

[21] J. P. Mottershead, K. Schmierer, M. Clemence, J. S. Thornton, F. Scaravilli, G. J. Barker, J. Newcombe, M. L. Cuzner, R. J. Ordidge, W. I. McDonald, and D. H. Miller, "High field MRI correlates of myelin content and axonal density in multiple sclerosis," *J. Neurol.*, vol. 250, pp. 1293–1301, 2003.

[22] G. Bartzokis, J. L. Cummings, D. Sultzer, V. W. Henderson, K. H. Nuechterlein, and J. Mintz, "White matter structural integrity in healthy aging adults and patients with Alzheimer disease," *Arch. Neurol.*, vol. 60, pp. 393–398, 2003.

[23] D. D. Blatter, E. R. Bigler, S. D. Gale, S. C. Johnson, C. V. Anderson, B. M. Burnett, N. Parker, S. Kurth, and S. D. Horn, "Quantitative volumetric analysis of brain MR: Normative database spanning 5 decades of life," *Amer. J. Neuroradiol.*, vol. 16, pp. 241–251, 1995.

[24] C. Davatzikos and S. M. Reznik, "Degenerative age changes in white matter connectivity visualized *in vivo* using magnetic resonance imaging," *Cereb. Cortex*, vol. 12, pp. 767–771, 2002.

[25] F. Kruggel, "MRI-based volumetry of head compartments: Normative values of healthy adults," *NeuroImage*, vol. 30, pp. 1–11, 2006.
[26] A. Pfefferbaum, E. V. Sullivan, M. Hedehus, K. O. Lim, E. Adalsteinsson, and M. Moseley, "Age-related decline in brain white matter anisotropy measured with spatially correlated echo-planar diffusion tensor imaging," *Magn. Reson. Med.*, vol. 44, pp. 259–268, 2000.
[27] U. C. Wieshmann, M. R. Symms, G. J. Parker, C. A. Clark, L. Lemieux, G. J. Barker, and S. D. Shorvon, "Diffusion tensor imaging demonstrates deviation of fibers in normal appearing white matter adjacent to a brain tumor," *J. Neurol. Neurosurg. Psychiatry*, vol. 68, pp. 501–503, 2000.
[28] T. L. Kemper, "Neuroanatomical and neuropathological changes during aging and dementia," in *Clin. Neurol. Aging*, M. L. Albert and J. E. Knoefel, Eds., 2nd ed. New York: Oxford Univ. Press, 1994, pp. 3–67.
[29] F. Fazekas, R. Schmidt, and P. Scheltens, "Pathophysiologic mechanisms in the development of age-related white matter changes of the brain," *Dementia Geriatric Disorders*, vol. 9, pp. 2–5, 1998.
[30] E. Englund, A. Brun, and C. Alling, "White matter changes in dementia of Alzheimer's type: Biochemical and neuropathological correlates," *Brain*, vol. 111, pp. 1425–1439, 1988.
[31] T. Erkinjuntti, O. Benavente, M. Eliasziw, D. G. Munoz, R. Sulkava, M. Haltia, and V. Hachinski, "Diffuse vacuolization (spongiosis) and arteriolosclerosis in the frontal white matter occurs in vascular dementia," *Arch. Neurol.*, vol. 53, pp. 325–332, 1996.
[32] J. Rademacher, V. Engelbrecht, U. Buergel, H.-J. Freund, and K. Zilles, "Measuring *in vivo* myelination of human white matter fiber tracts with magnetization transfer MR," *NeuroImage*, vol. 9, pp. 393–406, 1999.